Top-down fabrication of GaN nano-laser arrays by displacement Talbot lithography and selective area sublimation

Benjamin Damilano, Pierre-Marie Coulon, Stephane Vézian, Virginie Brandli, Jean-Yves Duboz, Jean Massies, Philip Shields

Applied Physics Express

LETTER • **OPEN ACCESS**

Top-down fabrication of GaN nano-laser arrays by displacement Talbot lithography and selective area sublimation

OPEN ACCESS

Applied Physics Express 12, 045007 (2019) LETTER

https://doi.org/10.7567/1882-0786/ab0d32

Top-down fabrication of GaN nano-laser arrays by displacement Talbot lithography and selective area sublimation

Benjamin Damilano[1*], Pierre-Marie Coulon[2], Stéphane Vézian[1], Virginie Brändli[1], Jean-Yves Duboz[1], Jean Massies[1], and Philip A. Shields[2]

[1]Université Côte d'Azur, CNRS, CRHEA, Valbonne, France
[2]Dept. Electrical & Electronic Engineering, University of Bath, Bath, BA2 7AY, UK, United Kingdom

*E-mail: bd@crhea.cnrs.fr

Received December 30, 2018; revised February 28, 2019; accepted March 6, 2019; published online March 27, 2019

We show that a 4 μm thick GaN layer grown by metal-organic vapour phase epitaxy can be transformed into a well-organized array of GaN nanowires (NWs) using displacement Talbot lithography and selective area sublimation. The optical quality of the GaN NWs obtained by this method is attested by their room temperature photoluminescence and the observation of lasing under optical pumping with a minimum excitation power density threshold of 2.4 MW cm^{-2}. © 2019 The Japan Society of Applied Physics

The fabrication of nanolaser arrays is currently required by the development of nanophotonics for various applications such as imaging system displays[1)] or optical interconnects.[2–4)] This crucial need has recently given rise to a lot of work aiming to achieve direct band-gap semiconductor nanowire (NW) arrays, where each NW can act as both the gain medium and the optical cavity. In particular, much work has been devoted to arrays of free standing vertical GaN NW, mainly because of the resounding industrial success of GaN and its alloys for producing green, blue, UV, and finally white light emitting diodes and blue lasers.[5)] Actually, there are already several papers reporting optically pumped single-mode laser operation of single GaN NWs.[6–12)] As for other semiconductors, two main routes are followed to get GaN NW arrays, generally termed as *top-down* and *bottom-up* approaches. The first one uses the powerful technological toolbox developed for the semiconductor industry: in brief, lithography masking of the two-dimensional (2D) epitaxial GaN layer to define the NW array geometry, and dry or/and wet-etching to finally obtain well isolated vertical NWs of well controlled length and diameter.[13)] The second has a more recent origin and clearly corresponds to a rupture in the classical 2D epitaxial crystal growth procedure on a given single-crystal substrate. Indeed, it relies on unusual nucleation and growth procedures such as the vapor–liquid–solid epitaxial process, which favor the local *self-organized* 1D epitaxial growth of NWs on the locally modified surface of a host substrate,[14)] or the selective growth on a mask, using a lithography process as for the top-down approach.[15,16)] As usual, each of these approaches has advantages and drawbacks. The main advantage of using *top-down* instead of *bottom-up* approaches is that the NW definition results from a post-growth process applied on a 2D classical epitaxial structure grown onto a substrate by various well-established semiconductor growth methods, such as metal-organic chemical vapor deposition (MOCVD) or molecular beam epitaxy (MBE). This ensures well controlled heterostructure parameters, such as thicknesses and doping levels of the different epitaxial layers, including quantum well or quantum dot layers, and roughness at the different interfaces. The main drawback is that the generally used dry etching techniques, such as reactive ion etching or inductively coupled plasma, provoke ion-induced surface defects increasing the surface recombination of carriers, affecting the luminescence efficiency of the NWs. Obviously, such a detrimental effect increases with the nanostructure surface-to-volume ratio. However, it should be noted that recently, by using a dry etching process followed by wet-etching to smooth the GaN NW sidewalls and control their diameter, NW single-mode laser emissions have been reported.[9,11,12)] Note that in Ref. 12, optical pumping was performed on the vertical NW, while most publications refer to optical pumping on a single NW extracted from the NW array and placed horizontally on a host substrate (Refs. 3–11), i.e. excited along its length, which leads to an uniform absorption and pumping in the NW and thus to a lower laser threshold. Although most of the papers reporting GaN NW laser action correspond to a bottom up NW fabrication (Refs. 1–7), these last results build confidence in top down approaches providing that special attention is taken to preserve the NW surface.

We have previously shown that high-quality low-dimensional (diameter of few nanometers) GaN and GaN/(Ga,In)N NWs can be fully made in situ by a simple low-cost top-down method making use of the congruent nature of GaN evaporation (sublimation), and termed as selective area sublimation (SAS).[17,18)] Once a mask of refractory material such as Si_3N_4 or SiO_2 is deposited on the GaN surface, a single-step of high-temperature thermal annealing is performed under high-vacuum, resulting in the GaN sublimation in places uncovered by the mask. GaN sublimation by high-temperature annealing under vacuum has been clearly evidenced by reflection high-energy electron diffraction intensity oscillations and laser reflectivity experiments.[19–21)] Here, we report a top-down approach combining SAS with a newly developed low-cost, fast and large-scale process for patterning, the so-called displacement Talbot lithography (DTL).[22,23)]

The samples were grown on 2 inch c-plane (0001) sapphire substrates by MOCVD in a 7 × 2 inch close-coupled showerhead Aixtron reactor. A 2 μm non-intentionally doped GaN was first grown followed by a 2 μm Si- doped (5×10^{18} cm^{-3}) GaN layer. The first 2 μm of GaN are undoped in order to favour the coalescence of the layer after

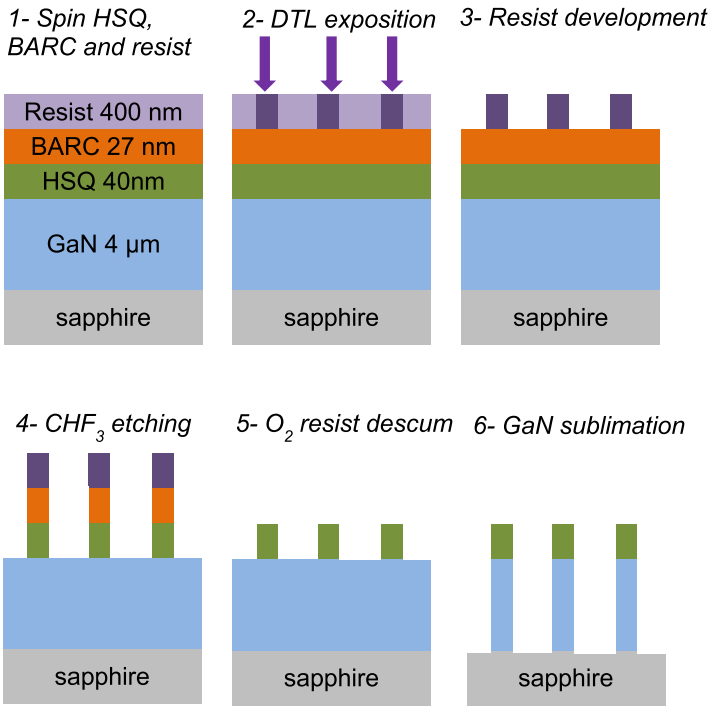

Fig. 1. (Color online) Process steps used for the fabrication of the nanowire arrays. 1—Deposition of a 40 nm hydrogen silsesquioxane (HSQ) layer, a 27 nm bottom antireflective coating (BARC) and a 400 nm photosensitive resist. 2—Exposition to the displacement Talbot lithography system with a 375 nm illumination source through an optical mask consisting of 800 nm diameter holes in a hexagonal arrangement with a 1.5 μm pitch. 3—Resist development. 4—CHF_3 plasma etching. 5—O_2 plasma descum of the resist. 6—GaN sublimation under vacuum in a molecular beam epitaxy chamber.

an initial 3D growth mode. The threading dislocation density emerging at the surface was evaluated from atomic force microscopy images[24] to be in the 3–4 $\times$ 10^8 cm^{-2} range, a typical value for standard MOCVD GaN templates on sapphire. One GaN sample was kept as a reference and another one was used for the top-down fabrication of GaN NWs with two different diameters. The process is detailed in Fig. 1. First, a 40 nm thick hydrogen silsesquioxane was spin coated on the full 2 inch wafer followed by a 270 nm bottom antireflective coating and a 400 nm photosensitive resist. Then, the sample was exposed with the DTL system (EULITHA PhableR 100, 375 nm illumination source with a power density of 1 mW cm^{-2}) through an optical mask consisting of 800 nm diameter holes in a hexagonal arrangement with a 1.5 μm pitch.[23] Two different doses of 220 and 240 mJ were used on two different regions (surface corresponding to a 1/4 2 inch each) of the sample. After resist development, CHF_3 plasma etching, and O_2 plasma descum, SiO_x nanodots with respective diameters of 330 and 360 nm are formed [top view SEM images of these dots are shown in the insets of Figs. 2(a) and 2(b), respectively]. Then, the SiO_x patterned GaN surface is submitted to the SAS process[17,18] performed at 940 °C under high-vacuum in a MBE chamber during 10 h.

After SAS etching, SEM shows [Figs. 2(a) and 2(b)] that well-defined hexagonal arrays of vertical NW of 4 μm length standing on the sapphire substrate are formed. As measured from top view SEM images after chemical etching of the SiO_x nanomask (not shown), NWs of 169 ± 31 and 219 ± 28 nm mean diameter are obtained for initial mask diameters of 330 and 360 nm, respectively. While in our

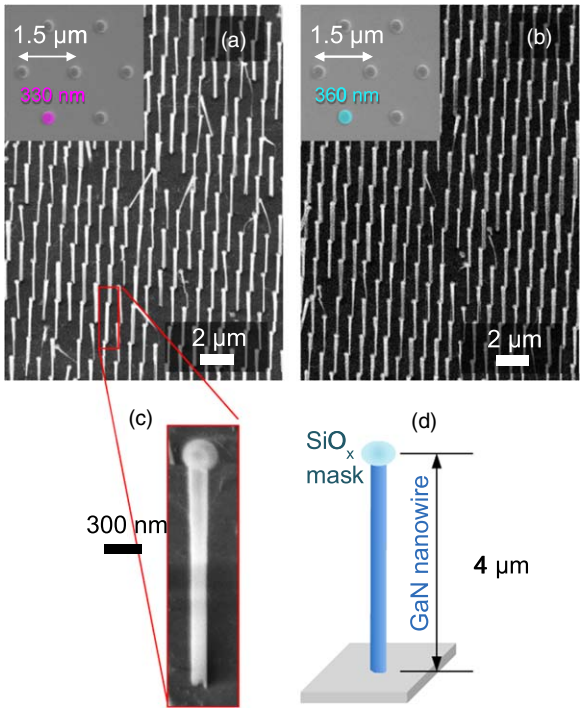

Fig. 2. (Color online) Scanning electron microscopy images in a tilted view (30°) of GaN nanowires made by selective area sublimation using a mask composed of SiO_x dots with a diameter of 330 nm (a) or 360 nm (b). The insets show scanning electron microscopy images in plan-view of the same samples before the sublimation process where we can see the dots of SiO_x with a diameter of 330 or 360 nm on top of the GaN surface. (c) Higher magnification scanning electron microscopy image in a tilted view (30°) of one GaN nanowire. (d) Corresponding schematics of one GaN nanowire standing on the sapphire substrate with the top SiO_x dot mask.

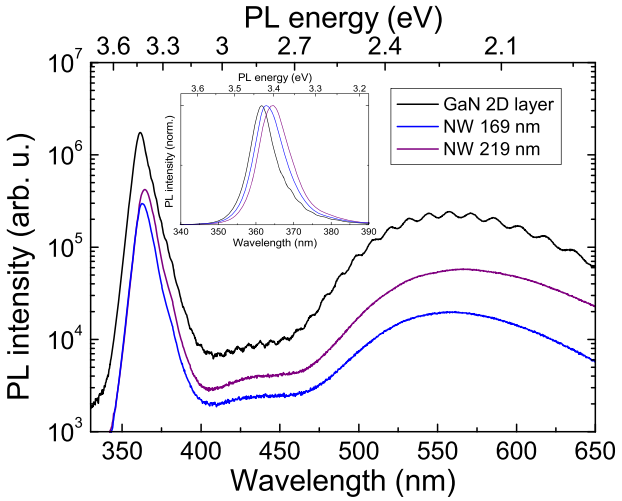

Fig. 3. (Color online) Room temperature photoluminescence using the 244 nm line of a CW frequency-doubled Ar laser of the GaN 2D layer and of the nanowire arrays with nanowire diameters of 169 and 219 nm. The inset shows the normalized photoluminescence spectra of the GaN band-edge.

previous works (Refs. 17 and 18) the height of the NWs obtained by SAS was intentionally restricted to ~100 nm, the present results clearly indicate that SAS is not limited to the fabrication of short length NWs since the NW height here is increased by a factor 40 to reach 4 μm [Figs. 2(c) and 2(d)]. It should also be noted that the diameter of the SiO_x nanomask is not significantly changed after sublimation [Fig. 2(c)]. This shows the perfect selectivity of the sublimation process between GaN and SiO_x. By subtracting the mean GaN NW radius from the initial mask radius we can deduce that the lateral sublimation of GaN reaches 81 (71) nm for the smallest (largest) NWs. By comparing this lateral sublimation with the vertical one we can estimate that the lateral/vertical sublimation ratio is about 2%. This value is significant for NW heights >1 μm and this lateral sublimation rate has to be taken into account in the initial mask design to obtain the final targeted NW diameter.

The photoluminescence (PL) experiments were performed at room temperature using a CW frequency-doubled Ar laser at 244 nm with a spot diameter of 120 μm and an excitation power of 30 mW. A pulsed 266 nm quadrupled Nd:YAG laser (400 ps/7 kHz) focused to a 2 μm spot diameter with a variable output power was also used.

In Fig. 3 are reported both the 300 K PL of the 4 μm thick GaN 2D layer before SAS and of the GaN NW arrays. The first observation is that the PL intensity of the 2D layer is a factor 5.9 and 4.2 higher than the one of the ensemble of NWs of diameter 169 and 219 nm, respectively. However, as the excitation laser spot diameter is much larger than the pitch, the NW PL intensity should be corrected by the NW filling factor. As the wavelength is much smaller than the pitch, we can neglect optical resonances and assume a uniform illumination. The filling factor is given by $\frac{2\pi}{\sqrt{3}}\left(\frac{r}{p}\right)^2$ where r and p are the NW radius and pitch respectively. This filling factor equals 1.6%–2.8% for small and large NWs respectively. The NW/2D layer PL ratio normalized by the filling factor now becomes 10.6 and 8.5 for small and large NWs respectively, showing that the PL efficiency of NWs is about 10 times higher than the one in 2D GaN. This can be mainly explained by a higher extraction efficiency of the GaN NW compared to a bare 2D GaN surface. Indeed, it has been shown by calculation that the light extraction efficiency of GaN NWs on silicon substrate into air can be larger than 65% for low filling factor (below 0.01 in our case) while it is only 4% for a 2D GaN layer.[25] The extraction roughly accounts for the observed luminescence ratio of 10. The second observation is about the PL peak energy: it is 3.431 eV for the 2D GaN which indicates a compressive strain, classically due to the difference of thermal expansion coefficient between sapphire and GaN, while the PL peak for the NW array is at smaller energy (3.415 eV and 3.405 eV for NW diameters of 219 and 169 nm, respectively) showing that the initial compressive stress of the 2D GaN layer is relaxed at least partially, as expected from strain relaxation by the free edges of the NWs. The strain can be deduced from the PL peak energy of the GaN band-edge considering a deformation potential of −8.5 eV.[26] This gives strain values of 0.25%, −0.06%, and 0.06% for the 2D GaN, the 219 and 169 nm diameter NWs, respectively, showing a similar behavior than top-down NWs fabricated using reactive ion etching.[27,28] A broad peak centered at 550–560 nm, the so-called yellow band characteristic of highly doped GaN layers is also observed. This band is structured by Fabry–Perot cavity oscillations for the 2D GaN layer. These oscillations are not visible for the NWs as expected, however the shape of this band is not significantly affected by the sublimation process.

The 300 K PL under pulsed excitation has been also studied using a μPL set-up with a spot laser diameter of 2 μm. According to the pitch of 1.5 μm, one single wire can be excited. Figures 4(a) and 4(b) shows the PL spectra as a function of the excitation power density. In the low excitation regime a broad PL spectrum (linewidth of 9–10 nm) is observed, while above a given threshold very sharp lines appear with a full width at half maximum down to 0.18 nm [insets in Figs. 4(a) and 4(b)].

The variation of the peak PL intensity as a function of the excitation power density in log scale shows the typical S-shape of a laser behavior with a superlinear increase of the PL intensity close to the laser threshold.[29] The lasing threshold is estimated to be 2.4 MW cm^{-2} for the 169 nm diameter NWs [Fig. 4(c)] and 4.9 MW cm^{-2} for the 219 nm diameter NWs [Fig. 4(d)]. The optical cavity is a Fabry–Perot resonator with a 4 μm thick GaN layer in between mirrors at the GaN/air and GaN/sapphire interfaces. On the PL spectra of Figs. 4(a) and 4(b) we can observe several optical modes. Their spacing is not constant with the wavelength as expected from a Fabry–Perot cavity. Close to a fixed wavelength of ~370 nm (excitation power density of 3.8 MW cm^{-2}), the mode spacing is 3.0 nm for the 169 nm diameter NWs [Fig. 4(a)] while it is 2.0 nm for the 219 nm diameter NWs [Fig. 4(b)]. The mode spacing $\Delta\lambda$ is given by:

$$\Delta\lambda = \frac{\lambda^2}{2L}\left(n - \lambda\frac{dn}{d\lambda}\right)^{-1}, \quad (1)$$

where λ is the wavelength, L the NW length, n the effective refractive index, and $dn/d\lambda$ the chromatic dispersion. The effective refractive index is expected to be lower in the case of the 169 nm diameter NWs due to their smaller diameter.[30] Therefore, the mode spacing decrease observed when the NW diameter increases is consistent with Eq. (1). The

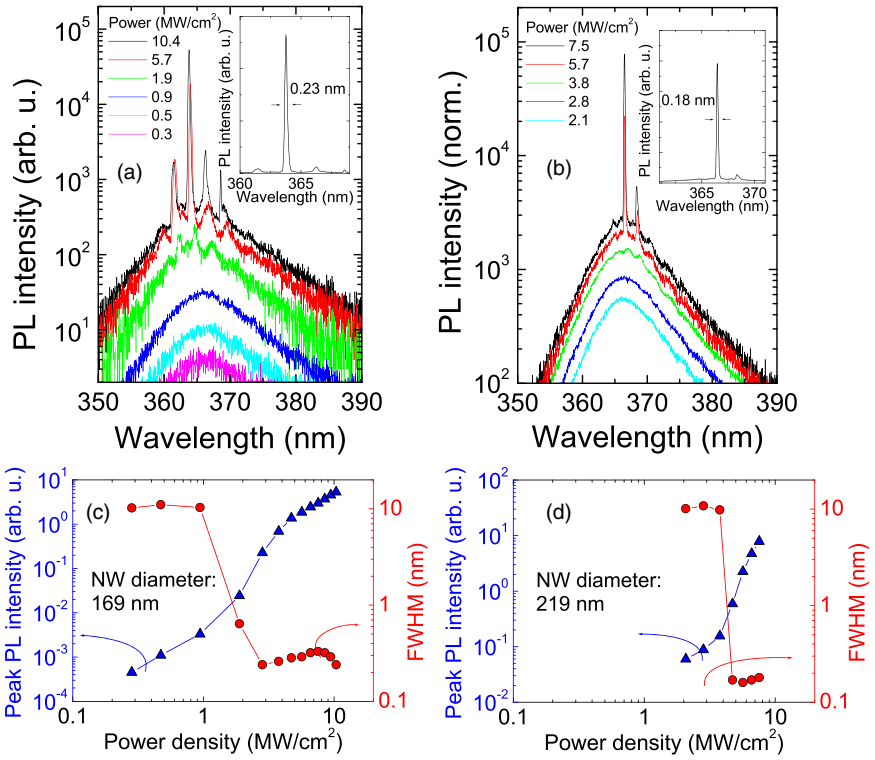

Fig. 4. (Color online) Room temperature micro-photoluminescence on single nanowires under pulsed laser excitation. Photoluminescence spectra in log scale of the samples with 169 nm (a) and 219 nm (b) nanowire diameters at different excitation power densities. The insets show the photoluminescence spectrum in linear scale for the highest excitation power density. (c) and (d) Peak photoluminescence intensities and full width at half maximum as a function of the excitation power density.

threshold values obtained are larger than those reported in (7) 22 kW cm^{-2} or (9) 231 kW cm^{-2}, but there is a strong difference in the excitation scheme since we are probing the standing NWs from the top while in both aforementioned references the NWs were broken and pumped from the side, in much more favourable conditions. Actually, these threshold values are comparable to those recently reported by Ref. 12 for GaN NWs obtained by a two-step top-down approach combining Cl_2 dry-etching and KOH wet-etching (minimum threshold of 3.31 MW cm^{-2}) and pumped from the top. In our case, we observe a lower lasing threshold of 2.4 MW cm^{-2} for the 169 nm diameter NWs. The reason of this reduced threshold compared to the 219 nm diameter NWs could be related to a better light injection for the smaller NW diameter due to their smaller effective refractive index.

In Figs. 4(c) and 4(d), we observe that the intensity ratio between above threshold and below threshold is not very large, of the order of 10. This ratio is related to the β factor of the laser (β varies as the inverse of this ratio). As NW efficiently collect emission along the NW even below threshold, they have a large β factor, and a value of 0.1 is realistic. We however agree that this experiment does not allow for a precise measurement of the β factor.

In conclusion, we have shown that DTL and SAS can be combined for wafer scale fabrication of arrays of GaN nanolasers. While in our previous reports SAS was used to form very short (100 nm) NWs, in the present work we fabricated GaN NWs with a length of 4 μm. The sublimation has the advantages of being a single-step process giving NWs showing a lasing effect at room temperature under optical pumping indicating very small damages at the surface of the NWs during the fabrication process.

Acknowledgments This work has been supported by the technology facility network RENATECH and the French National Research Agency (ANR) through the project NAPOLI (ANR-18-CE24-0022), and the "Investissements d'Avenir" program GaNeX (ANR-11-LABX-0014). It has also been supported by the Engineering & Physical Science Research Council, UK (EPSRC) (EP/M015181/1, EP/M022862/1). The authors would like to thank M. Leroux and J. Brault for the critical reading of the manuscript.

ORCID iDs Benjamin Damilano https://orcid.org/0000-0001-7127-4461 Philip A. Shields https://orcid.org/0000-0003-0517-132X

1) K. Kishino and S. Ishizawa, Appl. Phys. Lett. **109**, 71106 (2016).
2) S. Arafin, X. Liu, and Z. Mi, J. Nanophotonics **7**, 74599 (2013).
3) R. Röder, T. P. H. Sidiropoulos, C. Tessarek, S. Christiansen, R. F. Oulton, and C. Ronning, Nano Lett. **15**, 4637 (2015).
4) M. D. Brubaker, P. T. Blanchard, J. B. Schlager, A. W. Sanders, A. Roshko, S. M. Duff, J. M. Gray, V. M. Bright, N. A. Sanford, and K. A. Bertness, Nano Lett. **13**, 374 (2013).
5) S. Nakamura and G. Fasol, *The Blue Laser Diode* (Springer, Berlin, 1997).
6) J. C. Johnson, H.-J. Choi, K. P. Knutsen, R. D. Schaller, P. Yang, and R. J. Saykally, Nat. Mater. **1**, 106 (2002).
7) S. Gradečak, F. Qian, Y. Li, H.-G. Park, and C. M. Lieber, Appl. Phys. Lett. **87**, 173111 (2005).
8) M. Sakai, Y. Inose, K. Ema, T. Ohtsuki, H. Sekiguchi, A. Kikuchi, and K. Kishino, Appl. Phys. Lett. **97**, 151109 (2010).
9) Q. Li, J. B. Wright, W. W. Chow, T. S. Luk, I. Brener, L. F. Lester, and G. T. Wang, Opt. Express **20**, 17873 (2012).
10) H. Xu, J. B. Wright, T.-S. Luk, J. J. Figiel, K. Cross, L. F. Lester, G. Balakrishnan, G. T. Wang, I. Brener, and Q. Li, Appl. Phys. Lett. **101**, 113106 (2012).
11) C. Li et al., Nano Lett. **17**, 1049 (2017).
12) M. Behzadirad, M. Nami, N. Wostbrock, M. R. Zamani Kouhpanji, D. F. Feezell, S. R. J. Brueck, and T. Busani, ACS Nano **12**, 2373 (2018).
13) P. Shields, M. Hugues, J. Zúñiga-Pérez, M. Cooke, M. Dineen, W. Wang, F. Causa, and D. Allsopp, Phys. Status Solidi C **9**, 631 (2012).
14) M. Yoshizawa, A. Kikuchi, M. Mori, N. Fujita, and K. Kishino, Jpn. J. Appl. Phys. **36**, L459 (1997).
15) S. D. Hersee, X. Sun, and X. Wang, Nano Lett. **6**, 1808 (2006).
16) S. Li and A. Waag, J. Appl. Phys. **111**, 71101 (2012).

17) B. Damilano, S. Vézian, J. Brault, B. Alloing, and J. Massies, Nano Lett. **16**, 1863 (2016).
18) B. Damilano, S. Vézian, M. Portail, B. Alloing, J. Brault, A. Courville, V. Brändli, M. Leroux, and J. Massies, J. Cryst. Growth **477**, 262 (2017).
19) S. Fernández-Garrido, G. Koblmüller, E. Calleja, and J. S. Speck, J. Appl. Phys. **104**, 33541 (2008).
20) B. Damilano, J. Brault, and J. Massies, J. Appl. Phys. **118**, 24304 (2015).
21) N. Grandjean, J. Massies, F. Semond, S. Y. Karpov, and R. A. Talalaev, Appl. Phys. Lett. **74**, 1854 (1999).
22) H. H. Solak, C. Dais, and F. Clube, Opt. Express **19**, 10686 (2011).
23) P.-M. Coulon et al., Opt. Express **25**, 28246 (2017).
24) M. Khoury et al., Semicond. Sci. Technol. **28**, 35006 (2013).
25) M. Leroux, H. Lahrèche, F. Semond, M. Laügt, E. Feltin, N. Schnell, B. Beaumont, P. Gibart, and J. Massies, Mater. Sci. Forum **353–356**, 795 (2001).
26) M. Hugues, P. A. Shields, F. Sacconi, M. Mexis, M. Auf der Maur, M. Cooke, M. Dineen, A. Di Carlo, D. W. E. Allsopp, and J. Zúñiga-Pérez, J. Appl. Phys. **114**, 084307 (2013).
27) A. Kumar, M. Heilmann, M. Latzel, R. Kapoor, I. Sharma, M. Göbelt, S. H. Christiansen, V. Kumar, and R. Singh, Sci. Rep. **6**, 27553 (2016).
28) A.-L. Henneghien, G. Tourbot, B. Daudin, O. Lartigue, Y. Désières, and J.-M. Gérard, Opt. Express **19**, 527 (2011).
29) M. A. Zimmler, F. Capasso, S. Müller, and C. Ronning, Semicond. Sci. Technol. **25**, 24001 (2010).
30) C. Couteau, A. Larrue, C. Wilhelm, and C. Soci, Nanophotonics **4**, 90 (2015).